*Fracture Mechanics of Concrete and Concrete Structures -*
*Assessment, Durability, Monitoring and Retrofitting of Concrete Structures- B. H. Oh, et al. (eds)*
*ⓒ 2010 Korea Concrete Institute, Seoul, ISBN 978-89-5708-181-5*

# Numerical investigation on bond behavior of corroded reinforcement

C. Fischer & J. Ožbolt
*Institute of Construction Materials, University of Stuttgart, Germany*

C. Gehlen
*Centre for Building Materials, Technical University of Munich, Germany*

ABSTRACT: The paper presents the results of investigations obtained within the project B2 of the research group DFG FOR 537 "Modeling reinforcement corrosion". In the project the influence of corrosion on the interaction between steel and concrete is investigated. The experimental and numerical investigations are conducted on 'beam end' specimens. The paper presents the results of numerical investigations and their comparison with experimental results. The bond strength together with corresponding end displacement at reference state and different corrosion levels are modeled and compared with experimental results. Specimens without stirrups show strong reduction of bond strength with increase of corrosion level. In contrary to this, bond strength of specimens with stirrups is much less sensitive on the corrosion level of reinforcement. The numerical results are in good agreement with the experimental observations.

## 1 INTRODUCTION

The corrosion of steel in concrete is a serious cause for deterioration of concrete structures. The main reasons for the rebar corrosion are carbonation of the concrete cover and chloride ingress. Both yields the destruction of the steel securing oxide layer and thus corrosion may start. The rebar corrosion affects: (i) the steel, by reducing the bar diameter, (ii) the concrete, by cracking due to the volumetric expansion of the corrosion products and (iii) the interaction between steel and concrete due to the loss of bond. The third point, which is investigated in this paper, is influenced by the two former points. However, in most cases the cracking of concrete cover has more serious impact on bond than the reduction of bar diameter.

Bond strength of the investigated ribbed bars is activated in three stages. The first stage is the activation of the weak chemical bond between steel and concrete at very low stress level. The second stage is due to the bearing of the ribs and the surrounding concrete (mechanical interlock). At this stage, the reinforcing bar generates bursting forces consisting of compressive cone stresses and tensile hoop stresses in the vicinity of the concrete. Once the tension strength of concrete is reached, longitudinal cracks split the surrounding concrete. The last stage is controlled by friction between the rebar with concrete in the rib dales and the surrounding concrete. The bond strength is predominantly controlled by the ratio of concrete cover/bar diameter and the quality of concrete. The gradient of the loss of bond strength is controlled by confining pressure and/or confining reinforcement. The highest contribution to bond strength comes from the mechanical interlock. Bond failure due to cracking of the concrete cantilever, without cracking of concrete cover, is for corrosion endangered reinforcing bars not relevant.

Corrosion can affect bond strength of ribbed bars in several ways. The pressure due to volumetric expansion of the corrosion products may initially result in increasing bond strength – predominantly for plain bars. Once the tensile hoop stresses in the surrounding concrete exceed the tension strength, longitudinal cracks start to split the concrete cover and the bond strength is decreasing. As mentioned before, the controlling factor of bond strength becomes the confining reinforcement (FIB 2000).

The present paper is based on the results obtained in the framework of the research project which consists of an experimental and a numerical part. Within the experimental part the bond between steel and concrete is studied at a beam end specimen under accelerated corrosion by varying bar diameter, concrete cover and confining reinforcement. Within the numerical part the beam end specimen is simulated using finite elements (FE). Thus, a wide range of parametric studies with various concrete cover/bar diameter ratios, levels of confining reinforcement and corrosion levels are carried out.

The present paper shows the validation of the numerical model based on the performed experiments on the beam end specimen with two different concrete cover/bar diameter ratios, with and without stirrups and with different corrosion levels.

## 2 NUMERICAL MODEL

The 3D finite element code MASA was used to perform the numerical results presented in this paper. It was chosen because of the implemented realistic material model for concrete (microplane model) and the implemented discrete bond model.

The microplane model is used for three-dimensional damage and fracture analysis of concrete and reinforced concrete structures in the framework of the smeared crack approach. In the model the material is characterized by a relation between the stress and strain components on planes of various orientations. These planes may be imagined to represent the damage planes or weak planes in the microstructure, such as contact layers between aggregate pieces in concrete. The used microplane model is discussed in detail by Ožbolt et al. (2001).

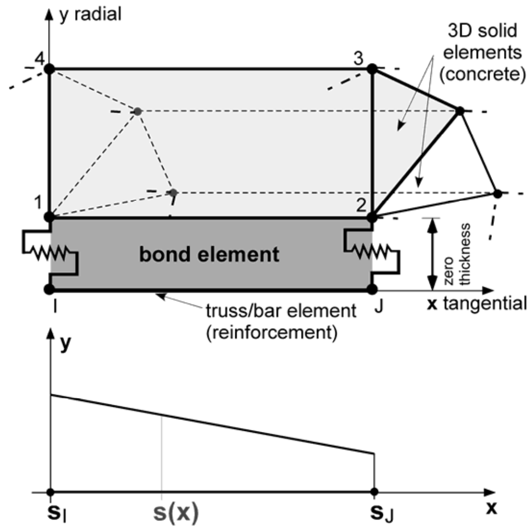

Figure 1. Schematic bond element and element displacement field (Ožbolt 2002).

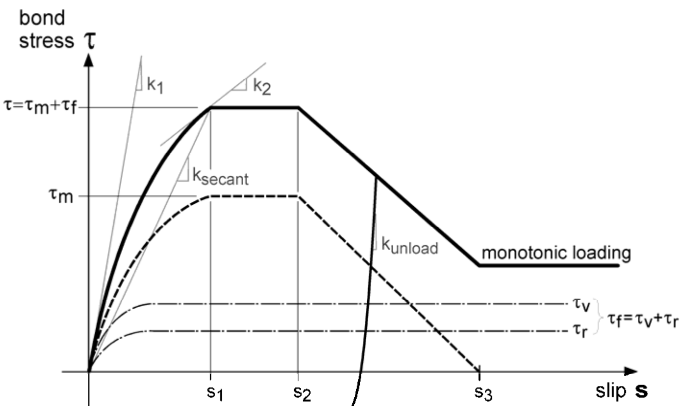

Figure 2. Stress-slip relation of the bond element model (Ožbolt 2002).

The discrete bond model allows bond characteristics to be defined by bond stress-slip curves. For this purpose 1D bar elements (reinforcement) are connected to surrounding 3D solid elements (see Fig. 1). Only the degree of freedom in bar direction (slip) is considered. The connection with the surrounding solid elements perpendicular to the bar direction is assumed to be perfect. By pulling out a ribbed bar tangential stresses parallel and radial stresses perpendicular to the bar axis are generated. The interaction between tangential and radial stresses works in two directions – from the solid elements to the bar elements and vice versa. A higher radial stress state in solid elements (compressive stress) causes a higher shear stress at the bar/solid interface. Furthermore, higher shear stress at the interface (higher bond strength due to a larger related rib area) causes higher tangential stresses in the surrounding solid concrete elements. Thus, different failure modes (pullout or splitting) are automatically accounted by the model (Ožbolt 2002).

The load transfer between reinforcement and concrete is accomplished through bearing of the reinforcement ribs on the surrounding concrete and through friction. The total bond resistance can be divided into two components: (i) a mechanical interlock $\tau_m$ and (ii) a friction component $\tau_f$ (see Figure 2). These components represent the bond stress for the case of no confining pressure, no damage and assuming elastic state of reinforcing steel. To account for the influences on bond strength from stress-strain state of the steel and the surrounding concrete, the factor Ω was introduced, which is calculated as:

$$\Omega = \Omega_s \cdot \Omega_c \cdot \Omega_{cyc} \tag{1}$$

where $\Omega_s$ controls the influence of the steel strain on the bond response, $\Omega_c$ controls the influence of the stress state in concrete and $\Omega_{cyc}$ accounts for the effect of loading-unloading-reloading on bond response. Factor $\Omega_c$ is calculated within a cylinder around 1D bar elements (Ožbolt 2002). The diameter of the cylinder is related to the actual bar diameter and consists of 3D linear elastic hexahedron elements with the modulus of elasticity of concrete (see Figure 3a). These elements represent the actual geometrical dimension of the rebar. In combination with 1D bar elements they have mechanical properties of steel. Thus, the modulus of elasticity is divided into $E_{bar}$ = 175 GPa and $E_{cylinder}$ = 30 GPa. Note that axial strength and bond resistance are attributed to the bar elements.

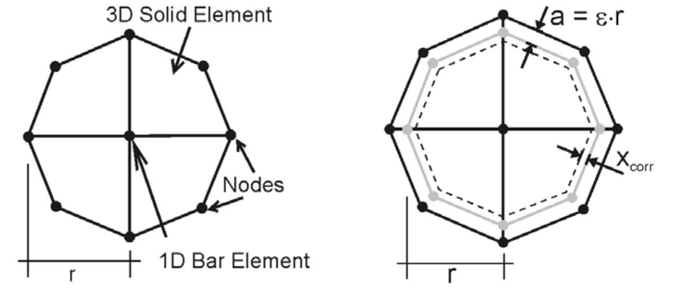


a b

Figure 3. Cross section of bar element (reinforcement) and surrounding solid elements (a) and corrosion expansion (b).

Corrosion is modeled by radial expansion of the linear elastic solid elements, which are connected to the bar elements (see Figure 3b). Due to the expansion of the cylinder, a compressive stress state and tensile hoop stresses are induced in the adjacent nonlinear elastic concrete elements. The controlling factor here is the tensile strength of concrete. As soon as the tensile stress reaches the tensile strength, cracks start to grow through the concrete cover.

The expansion is derived by the aid of a 2D xy-linear expansion function with the following formula:

$$a = -r + \sqrt{r^2 + (\nu - 1)\cdot(2rx - x^2)} \tag{2}$$

with

$r$ = uncorroded steel radius [mm]
$x$ = penetration depth [mm]
$a$ = free radius increase of original radius [mm]
$\nu$ = volume factor between corrosion products and consumed steel [-]

According to a literature review (Coronelli 2002), the volume factor is set to $\nu = 2.0$. For the sake of simplicity no corrosion layer was modeled. Expansion is introduced through radial expansion of 3D elements. The obtained increase of radius $a$ is the so called free radius increase since the formula does not take into account the boundary action of the surrounding concrete elements. The actual increase in radius is affected by the modulus of elasticity of the linear elastic solid elements $E_{cylinder} = 30$ GPa and the stiffness of the surrounding concrete elements. However, so far there is no founded information about the modulus of elasticity of the corrosion products. It is due to the fact that there is no information on the amount of corrosion products that migrates into the radial cracks around the reinforcement bar. This might cause differences between numerical and experimental results.

## 3 SPECIMEN AND DISCRETIZATION

The beam end specimen with four bars placed in the corners is chosen according to the test method proposed by Chana (1990), see Figure 4. The height is reduced to 200 mm to obtain a square cross section of 200 x 200 mm$^2$. Different bond length and bond arrangements were simulated numerically. The present specimen has shown to be the optimal choice. Namely, the optimization of the specimen geometry was focused on not to reach the yield strength of steel as well as to get such crack development for which all four bars of one specimen can be pulled out without disturbing each other. The horizontal support at the pullout face of the specimen has a height of 100 mm whereas the vertical support is 90 mm wide and is placed at the rear top. At this position the bar is covered by a plastic sleeve to avoid an enhancement of the bond strength due to the vertical support forces.

The calculations are performed with four different specimen types (see Table 1). Each type is calculated without expansion (reference calculation) as well as with different expansion values (see Table 4). The expansion is applied before the application of the pullout load. The material parameters used are shown in Table 2. The concrete properties were tested for w/c = 0.5 with 360 kg/m$^3$ cement and with 8 mm maximum aggregate size. The bond parameters are derived from pull out tests of uncorroded (reference) beam end specimens (see Table 3).

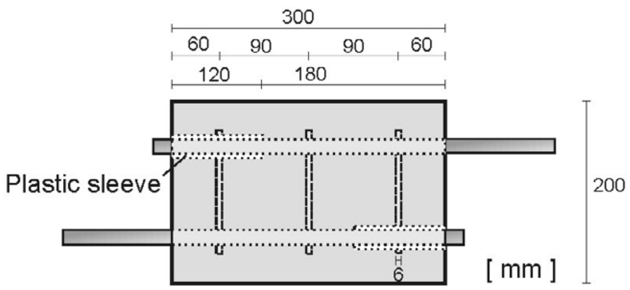


Figure 4. Cross section of specimen with stirrups.

Table 1. Specimen types.

| Type No. | d mm | c mm | c/d - | Stirrups mm |
|---|---|---|---|---|
| 1 | 12 | 20 | 1.67 | - |
| 2 | 12 | 20 | 1.67 | 6/90 |
| 3 | 16 | 35 | 2.19 | - |
| 4 | 16 | 35 | 2.19 | 6/90 |

Table 2. Input values of concrete and steel for the FE model.

| Concrete | | | | Steel | |
|---|---|---|---|---|---|
| $f_{cm}$ | $f_{ctm}$ | E | $G_f$ | $f_y$ | $R_m$ |
| MPa | MPa | MPa | N/mm | MPa | MPa |
| 35.0 | 2.6 | 29,300 | 0.08 | 500 | 600 |

Table 3. Input values of bond for the FE model.

| Bond | | | | | | | |
|---|---|---|---|---|---|---|---|
| $k_{sec}$ | $k_1$ | $k_2$ | R | $s_2$ | $s_3$ | $\tau_m$ | $\tau_f$ |
| N/mm | N/mm | N/mm | - | mm | mm | MPa | MPa |
| 600 | 1200 | 5.0 | 5.0 | 0.3 | 7.0 | 7.0 | 2.0 |

Table 4. Corrosion penetration depths x with corresponding expansion rates ε and crack width ranges according to corrosion product to parent metal volume ratio of two.

| $d_s$ | x | a | ε | $w_{type\ 1/3}$* | $w_{type\ 2/4}$** |
|---|---|---|---|---|---|
| mm | mm | mm | mm | mm | mm |
| 12 | 0.030 | 0.030 | 4.98E-03 | 0.12 | 0.11 |
| 12 | 0.040 | 0.040 | 6.62E-03 | 0.18 | 0.14 |
| 12 | 0.050 | 0.050 | 8.26E-03 | 0.22 | 0.18 |
| 12 | 0.075 | 0.074 | 1.23E-02 | 0.32 | 0.25 |
| 12 | 0.100 | 0.098 | 1.64E-02 | 0.40 | 0.33 |
| 12 | 0.125 | 0.122 | 2.04E-02 | 0.52 | 0.39 |
| 12 | 0.150 | 0.146 | 2.44E-02 | 0.62 | 0.48 |
| 12 | 0.175 | 0.170 | 2.83E-02 | 0.72 | - |
| 16 | 0.030 | 0.030 | 3.74E-03 | 0.05 | 0.09 |
| 16 | 0.040 | 0.040 | 4.98E-03 | 0.14 | 0.14 |
| 16 | 0.050 | 0.050 | 6.21E-03 | 0.19 | 0.19 |
| 16 | 0.075 | 0.074 | 9.29E-03 | 0.30 | 0.29 |
| 16 | 0.100 | 0.099 | 1.23E-02 | 0.39 | 0.38 |
| 16 | 0.125 | 0.123 | 1.54E-02 | 0.52 | 0.48 |
| 16 | 0.150 | 0.147 | 1.84E-02 | 0.65 | 0.56 |
| 16 | 0.175 | 0.171 | 2.14E-02 | 0.71 | 0.62 |
| 16 | 0.200 | 0.195 | 2.44E-02 | 0.83 | 0.71 |

w*- average crack width of specimens without stirrups
w**- average crack width of specimens with stirrups

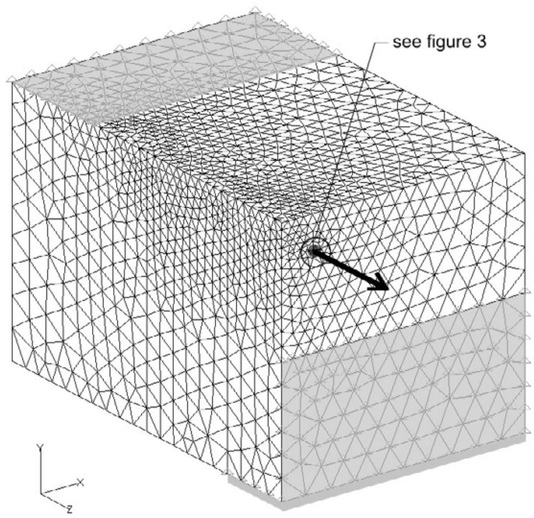


Figure 5. Finite element (FE) model with mesh, constraints and applied displacement direction.

The FE model, shown in Figure 5, contains one reinforcement bar, which is modeled along its bond length of 180 mm using 1D bar elements. Around these elements a cylinder of solid hexahedron elements with the actual bar diameter and linear elastic properties is arranged. With the aid of a 2D expansion function in the FE code, these elements were expanded to simulate different corrosion levels (see Table 4). The stirrups are modeled by 1D bar elements with rigid connection to the surrounding concrete elements.

## 4 RESULTS

The validation of the numerical model is accomplished by comparing numerical and experimental results for: (i) bond stress-end displacement curves, (ii) crack patterns and (iii) bond strength as a function of the increasing crack width that is due to the corrosion of reinforcement. The results of the bond stress-end displacement curves of the reference specimens type 1 to 4 are shown in Figures 6 to 9.

The displacement is measured as a relative value between the end of the bar and the concrete surface at the rear face of the specimen. All curves indicate that there is nearly no displacement of the bar end up to reaching bond strength. Furthermore, the bond stresses at peak load are far below bond strengths measured in RILEM pullout tests, which are around 16 MPa (Lettow 2006). This is because the failure is not due to pullout but it is caused by splitting of concrete cover.

By comparing the specimens without and with stirrups the trend to higher residual bond strengths with increasing displacement can be clearly seen (see Figs. 6-9). Furthermore, bond strengths are increasing by about 1 MPa due to the stirrups contribution. The numerical curves show less stiffer response than the experimentally obtained. However, regarding the bond strength and the displacement at bond strength good agreement is obtained.

Figure 10 shows the crack pattern of the type 1 specimen after corrosion expansion of $x = 30\ \mu m$, which induces a crack width of $w = 0.12$ mm. As in the experiments, only one crack develops through the concrete cover of a corner bar at low corrosion levels.

Figures 11 and 12 show numerical and experimental crack patterns of pre corroded type 1 specimens after bar pull out. In contrast to the analysis, in the experiment the corrosion crack develops at the side face instead of at the top face. This difference is due to the development of the crack that depends on the mesh which is randomly distributed in that area. The failure pattern partially follows the corrosion crack. However, final crack pattern is of the form of a cone break out. By comparing pull out crack patterns of different corrosion levels of one specimen type, nearly no differences could be found up to the observed crack widths of about 0.9 mm.

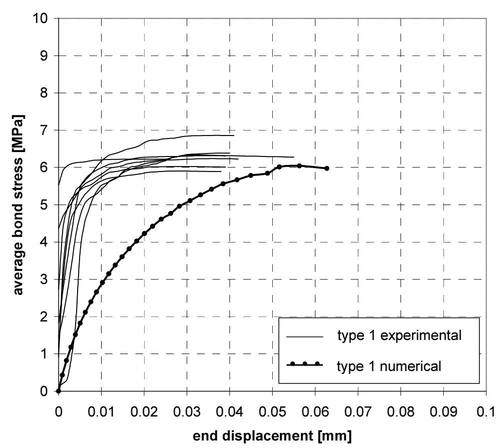


Figure 6. Comparison of experimental and numerical stress-displacement curves of type 1 reference specimens.

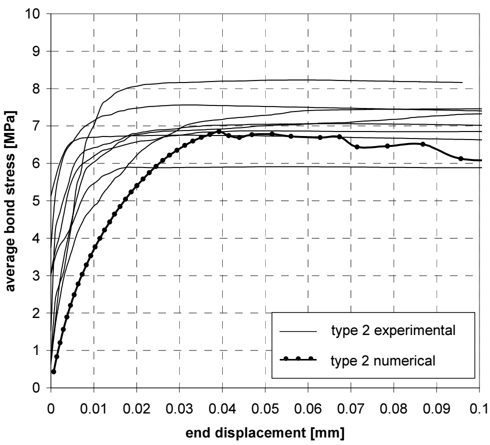


Figure 7. Comparison of experimental and numerical stress-displacement curves of type 2 reference specimens.

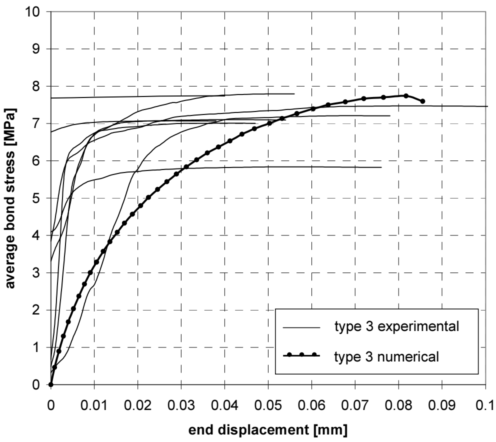


Figure 8. Comparison of experimental and numerical stress-displacement curves of type 3 reference specimens.

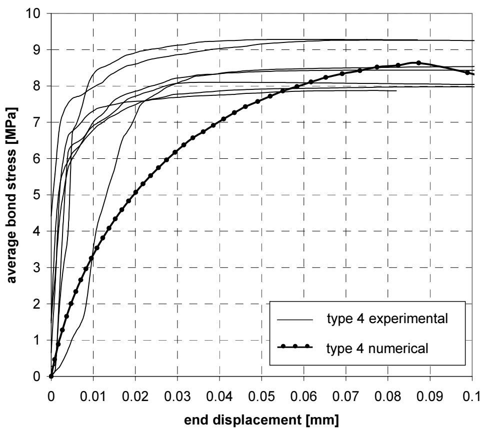


Figure 9. Comparison of experimental and numerical stress-displacement curves of type 4 reference specimens.

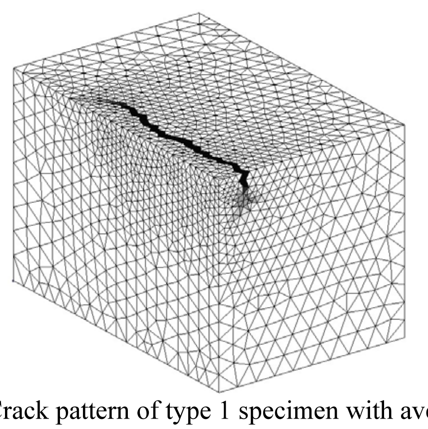

Figure 10. Crack pattern of type 1 specimen with average crack width of w = 0.12 mm without pullout.

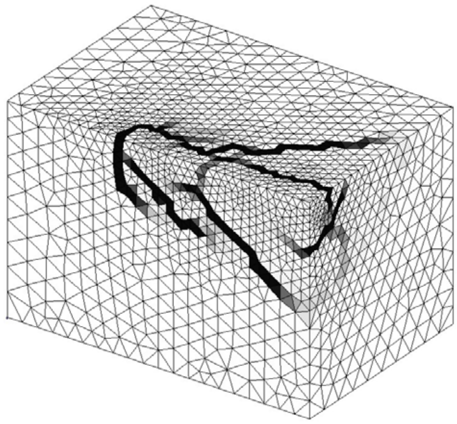

Figure 11. Crack pattern of type 1 specimen with an average crack width of w = 0.12 mm after maximum load of bar pullout.

Figure 12. Crack pattern of experimental type 1 specimen after maximum load of bar pull out.

By comparing numerically and experimentally obtained crack patterns for type 2 specimens, the influence of the stirrups becomes obvious (see Figs. 13-14). Due to its stiffness, the stirrups causes stress concentrations. Therefore, the long cone break-out (see Figs. 11-12) changes into a shorter but wider one. Nearly all specimens with stirrups have this wide break-out cone over the whole side (see Figure 14 on top face). In the numerical model the stirrups are modeled by 1D bar elements with no geometrical diameter in the mesh. This might be an explanation for the smaller front cone in numerical calculations (see Figure 13).

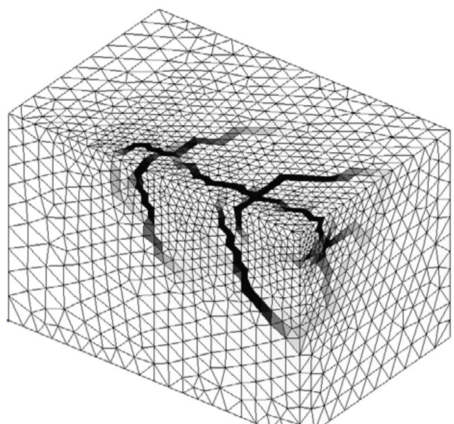

Figure 13. Crack pattern of type 2 specimen with an average crack width of w = 0.14 mm after maximum load of bar pull out.

Figure 14. Crack pattern of experimental type 2 specimen after maximum load of bar pull out.

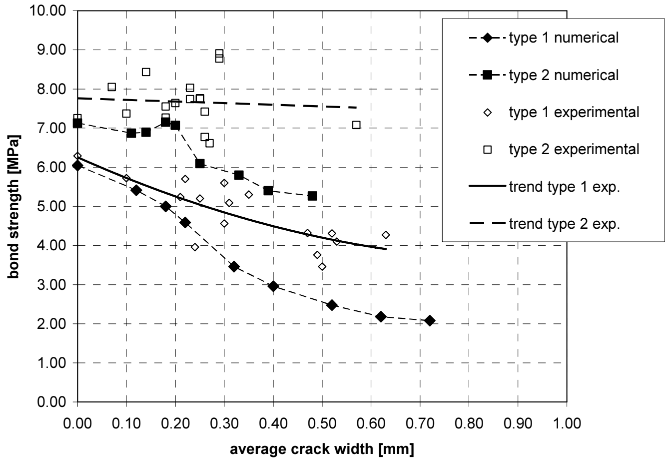


Figure 15. Bond strength over average crack width at different corrosion levels of specimen types 1 and 2.

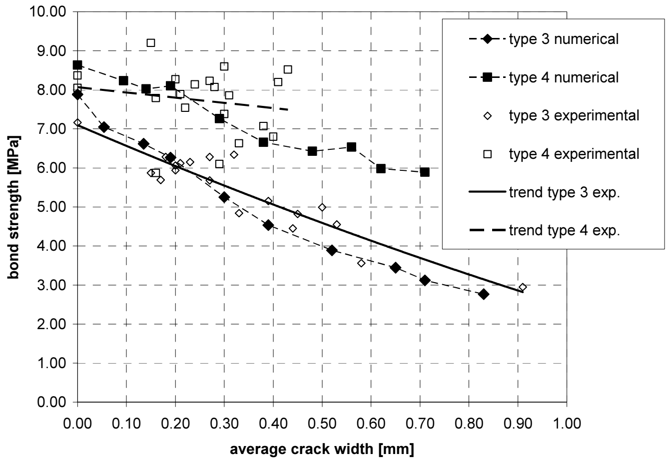


Figure 16. Bond strength over average crack width at different corrosion levels of specimen types 3 and 4.

The last point of the validation of numerical results is the comparison of the bond strength dependency on increasing crack width. Figure 15 shows this dependency for type 1 and 2 specimens. The numerical results for the type 1 specimen show good agreement with the experimental results up to the crack width of about 0.2 mm. From this point the numerically obtained bond strengths are decreasing faster than the experimentally obtained. Also, the numerical results for the type 2 specimens decrease faster than the experimentally measured bond strength after reaching a crack width of 0.2 mm. A possible reason could be the relatively small concrete cover, which is modeled by only three elements.

Another phenomenon which could not be found in the calculations is the slight increase in bond strength with increase of corrosion rate as experimentally observed on specimens with stirrups. The reason might be a higher friction between the rebar and the stirrups. This behavior is more distinctive at type 2 than type 4 specimens.

Figure 16 shows bond strength depending on crack width for type 3 and 4 specimens. The numerical results of type 3 specimen show a very good agreement with the experimental results up to the maximum observed crack width of around 0.9 mm. The type 4 model performs well up to the crack width of 0.2 mm. From this point there is a good agreement with only some experimental results. However, after the crack width of 0.2 mm the majority of the experimental results indicate a slower decreasing of bond strength than the numerical results.

The influence of stirrups is clearly visible for all specimen types and up to the crack width of 0.2 mm a very good agreement between experimental and numerical results can be seen.

## 5 CONCLUSION

The performed numerical studies for the beam end specimen on bond strength and failure mode show good agreement with experimental results. The validation of the bond-displacement relationship, the cracking pattern and the relationship between the bond strength and crack width are discussed. The numerically obtained bond stress-displacement curves turned out to be less stiffer than the experimental curves. However, the comparison between bond stress and bar end displacement at peak load show good agreement.

The numerically obtained crack patterns show good agreement with the experimentally obtained failure modes. Compared to specimens without stirrups, specimens with stirrups show higher residual bond strength and less influence of corrosion on bond resistance.

By comparing numerical and experimental results, regarding the bond strength dependency on the crack width, good results are obtained up to crack widths of 0.2 mm. With increasing crack width the numerical obtained bond strength is decreasing faster than the experimental one, except for type 3 specimens. Here a very good agreement is found up to maximum crack widths of about 0.9 mm. However, there are some effects studied at the experiments which are not reproduced numerically. For instance the slight increase of bond strength with increasing corrosion compared to the uncorroded reference specimens with stirrups.

The predicted failure mode in all cases is concrete splitting or concrete cone break out. Even at higher corrosion levels there is nearly no end slip at peak load.

The numerical and experimental results lead to the conclusion that for specimens without stirrups there is strong degradation of bond resistance with increase of crack width. On the contrary to this, bond strength of specimens with stirrups is much less sensitive to the corrosion of main reinforcement.

Finally it can be concluded that the performed numerical study at a beam end specimen with the aid of the 3D FE code MASA showed a good agreement with the experimental results obtained in the framework of the DFG research project “Bond behavior of corroded reinforcement”.

## ACKNOWLEDGEMENT

The paper based project is part of the DFG research group 537 “Modeling reinforcement corrosion”. The authors wish to thank the German Research Foundation (DFG) for founding this project and supporting the research issue.

## REFERENCES

Chana, P. S. 1990. A test method to establish realistic bond stresses. *Magazine of Concrete Research* 42(151): 83-90.

Coronelli, D. 2002. Corrosion cracking and bond strength modeling for corroded bars in reinforced concrete. *ACI Structural Journal* 99(3): 267-276.

FIB 2000. Bond of reinforcement in concrete. *State-of-the-art-report* Bulletin 10: 187-215.

Lettow, S. 2006. Ein Verbundelement für nichtlineare Fintite Elemente Analysen – Anwendung auf Übergreifungsstöße. PhD Thesis, Stuttgart.

Ožbolt, J.; Li, Y. & Kožar, I. 2001. Microplane model for concrete with relaxed kinematic constraint. *International Journal of Solids and Structures* 38: 2683-2711.

Ožbolt, J.; Lettow, S. & Kožar, I. 2002. Discrete bond element for 3D finite element analysis of reinforced concrete structures. In Balázs-Bartos-Cairns-Borosnyói (eds.), *Bond in Concrete – from research to standards; Proc. 3rd intern. symp.*. Budapest: University of Technology and Economics.